Chemistry–A European Journal
Research Article
doi.org/10.1002/chem.202400765
Chemistry Europe
European Chemical Societies Publishing
www.chemeurj.org

Dual Role of a Novel Heteroleptic Cu(I) Complex in Visible-Light-Driven CO_2 Reduction

Cecilia Bruschi,[a] Xin Gui,[b] Pascal Rauthe,[b] Olaf Fuhr,[c, d] Andreas-Neil Unterreiner,[b] Wim Klopper,[b, c] and Claudia Bizzarri*[a]

A novel mononuclear Cu(I) complex was synthesized *via* coordination with a benzoquinoxalin-2′-one-1,2,3-triazole chelating diimine and the bis[(2-diphenylphosphino)phenyl] ether (DPEPhos), to target a new and efficient photosensitizer for photocatalytic CO_2 reduction. The Cu(I) complex absorbs in the blue-green region of the visible spectrum, with a broad band having a maximum at 475 nm ($\varepsilon = 4500\ M^{-1}cm^{-1}$), which is assigned to the metal-to-ligand charge transfer (MLCT) transition from the Cu(I) to the benzoquinoxalin-2′-one moiety of the diimine. Surprisingly, photo-driven experiments for the CO_2 reduction showed that this complex can undergo a photo-induced electron transfer with a sacrificial electron donor and accumulate electrons on the diimine backbone. Photo-driven experiments in a CO_2 atmosphere revealed that this complex can not only act as a photosensitizer, when combined with an Fe(III)-porphyrin, but can also selectively produce CO from CO_2. Thus, owing to its charge-accumulation properties, the non-innocent benzoquinoxalin-2-one based ligand enabled the development of the first copper(I)-based photocatalyst for CO_2 reduction.

Introduction

Nature converts carbon dioxide into carbohydrates and other biomolecules by means of photosynthesis, storing the energy from the sun in new chemical bonds, employing water as an electron and proton donor.[1] Such a sustainable system is the Holy Grail of researchers, who strive to close the carbon cycle and turn CO_2 into valuable products.[2] In artificial photosynthesis, a photosensitizer (PS) undergoes a reductive quenching with a sacrificial electron donor (SeD) or an oxidative quenching with a catalyst (CAT), which is then reduced to activate CO_2.[3] In homogeneous photocatalysis, the distinguished molecular systems usually involve metal complexes with redox-active ligands, and only in limited cases organic compounds, mainly as PS.[4] The non-innocent ligands are often N-containing sp^2-hybridized heterocycles, employed to coordinate metal ions, forming PS and CAT. These ligands can be macrocycles,[5] multi- or bidentate molecules.[6] Bidentate Schiff bases or NN-chelating ligands are simply called "diimine" and are both σ-donors and π-acceptors. Earth-abundant metal-based photosensitizers[7] are often copper-based complexes,[8] with an oxidation state of +1. In those Cu(I) complexes, the lowest-unoccupied molecular orbital (LUMO) is often located on the diimine ligand, since the d-shell in Cu(I) is filled, thus the reduction processes are generally located in the diimine. As a consequence, the diimine is not only responsible of the potential values at which the copper complex is reduced, but also actively participates to the energetic lowest absorption of the electromagnetic radiation, which is formally an electron transfer from a metal-centered orbital to the first free π* orbital of the diimine. Thus, a metal-to-ligand charge-transfer (MLCT) state is populated. The energy value of the π*-orbital strongly influences the electrochemical and photophysical properties. For this reason, aiming at an efficient earth-abundant metal-based PS, an optimized engineering of the non-innocent ligand is necessary, so that the LUMO level of the final complex is low enough to allow the absorption in the visible region of the solar radiation, enabling at the same time a convenient electron transfer to a possible catalyst. Derivatives of 1,10-phenanthroline have been extensively used in this respect, to form efficient photosensitizers for photocatalytic CO_2 reduction or H_2 production.[9]

Less explored are heteroleptic Cu(I) complexes based on chelating diphosphines (PP) and asymmetric chelating diimines such as quinolyl- or quinoxalyl-1,2,3-triazole.[10] In these cases, the PP ligand is usually sterically hindered and has mainly a structural function, limiting the Jahn-Teller distortion Cu(I) complexes undergo in the excited state. On the diimine, the 1,2,3-triazole moiety has an ancillary function, which stabilizes the metal coordination, avoiding the formation of diimine homoleptic Cu complexes, while the benzofused 6-member *N*-heterocycle serves as an electron acceptor in photo(redox)

[a] Dr. C. Bruschi, Dr. C. Bizzarri
Institute of Organic Chemistry, Karlsruhe Institute of Technology, Kaiserstraße 12, 76131 Karlsruhe, Germany.
E-mail: bizzarri@kit.edu
[b] Dr. X. Gui, P. Rauthe, Prof. Dr. A.-N. Unterreiner, Prof. Dr. W. Klopper
Institute of Physical Chemistry, Karlsruhe Institute of Technology, Kaiserstraße 12, 76131 Karlsruhe, Germany
[c] Dr. O. Fuhr, Prof. Dr. W. Klopper
Institute of Nanotechnology, Karlsruhe Institute of Technology. Kaiserstraße 12, 76131 Karlsruhe, Germany
[d] Dr. O. Fuhr
Karlsruhe Nano Micro Facility (KNMFi), Karlsruhe Institute of Technology, Kaiserstraße 12, 76131 Karlsruhe, Germany

Supporting information for this article is available on the WWW under https://doi.org/10.1002/chem.202400765

processes. Aiming at new earth-abundant photosensitizers, we tailored our design further. In particular, we have targeted a novel Cu(I) complex that not only can serve as a photosensitizer, but also is able to interact with CO_2 and works as a molecular photocatalyst (PCat), where the functions of light-absorption and reduction catalyst are embedded in the same metal complex. Only few single-components have been used as PCat in photo-driven CO_2 reduction, and usually, they are restricted to precious 4d or 5d metals,[11] besides some iron and cobalt porphyrins.[12] Recently, a purpurin complex of copper in oxidation state +2 was shown to work as PCat at a high concentration of electron donor.[13] Other Cu(II) complexes known to reduce CO_2 have been used only in electrocatalysis.[14]

In this work, we present a new heteroleptic Cu(I) complex, based on the diimine 1-ethyl-3-(1′-benzyl-1′,2′,3′-triazol-4′-yl)-benzo[*g*]quinoxalin-2-one, which acts as non-innocent ligand, favoring the reduction of CO_2. Thus, to the best of our knowledge, this is the first photocatalyst based on Cu(I) that has been reported so far.

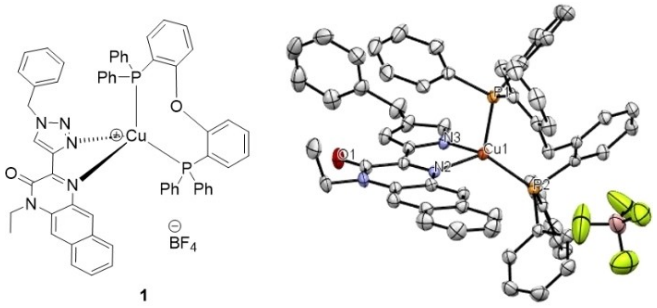

Figure 1. Left: chemical structure of the Cu(I) complex **1** investigated in this work. Right: ORTEP drawing of the molecular structure from X-ray diffraction. Hydrogen atoms and solvent molecules were omitted for clarity.

Results and Discussion

Synthesis and Molecular Structure

The new benzoquinoxalinone-based ligand was prepared in four steps with an overall yield of 43% (Scheme 1). The first step is a condensation reaction between 2,3-diaminonaphthalene **2** and the diketone **3**, carried out at 80 °C in a mixture of ethanol and glacial acetic acid in a ratio 7:3 in volume. The product, obtained with a yield of 76%, was subjected to an ethylation reaction with iodoethane in *N,N*-dimethylformamide (DMF), using potassium carbonate as a base. The tri(isopropyl)silyl protecting group (TIPS) was removed (yield 75%), so a copper-catalysed alkyne-azide cyclization (CuAAC) reaction followed, to give the final 1-ethyl-3-(1′-benzyl-1′,2′,3′-triazol-4′-yl)-benzo[g]quinoxalin-2-one (**BQXOT**) as a yellow powder in 92% of yield. This diimine was added in a dry dichloromethane (DCM) solution of tetrakis(acetonitrile)Cu(I) BF_4 and DPEPhos, under an argon atmosphere. The solution turned immediately from light yellow to vivid red. The coordination reaction stirred at room temperature for additional four hours. Then, the solvent was reduced by vacuum. When a layer of cyclohexane was gently juxtaposed, slow diffusion occurred overnight leading to the desired complex **1** formation of red crystals (yield 80%), which were suitable for X-ray analysis (Figure 1).

The suitable crystals for X-ray diffractometry were analyzed and refined and the structure shown in Figure 1 could be solved. The crystal system of **1** is monoclinic, belonging to the space group $P2_1/n$. The bond lengths between the copper core and the two coordinative nitrogen atoms of the **BQXOT** ligand are similar (Cu-N(2): 2.082 Å, Cu-N(3): 2.069 Å). Also the bond distances between the metal center and the coordinative P atoms of the DPEPhos ligand do not differ significantly (Cu-P(1): 2.278 Å, Cu-P(2): 2.214 Å). Lastly, the bite angles have a value of 79.54° for N(3)-Cu-N(2) and 115.32° for P(1)-Cu-P(2), suggesting a pseudo-tetrahedral geometry.

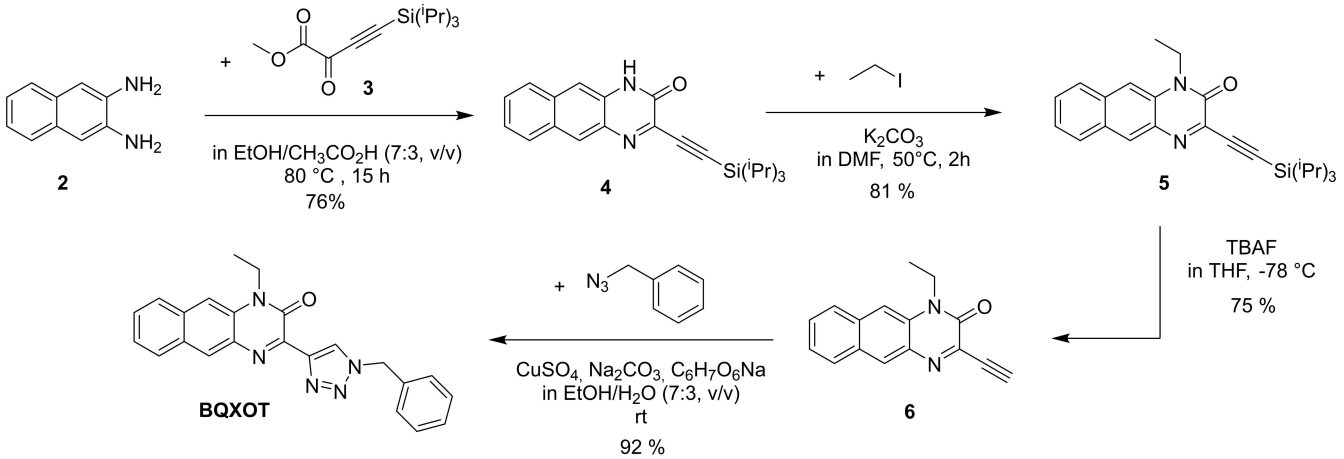

Scheme 1. Synthetic procedure for the preparation of the non-innocent ligand 1-ethyl-3-(1′-benzyl-1′,2′,3′-triazol-4′-yl)-benzoquinoxalin-2-one (**BQXOT**) used to coordinate Cu(I).

Photophysical and Electrochemical Characterization

UV-Vis absorption and emission of ligand **BQXOT** were recorded in DCM, while complex **1** was also investigated in DMF, since this is the solvent where we performed photocatalytic experiments (Figure 2). The most intense absorption bands occur within the UV region below 300 nm, where **BQXOT** and **1** have their maximum at around 240 nm in DCM. Interesting features are observed above 300 nm, where a structured band with three defined peaks at 340, 356, and 373 nm for **BQXOT** and at 360, 375, and 393 nm for complex **1** could be assigned to ligand-centered (^{1}LC) transitions. It is probable that an n-π* transition located on the carbonyl group contributes to this structured band, as similar shapes could be observed in quinone derivatives.[15]

In DMF, those peaks are less intense, with a different ratio among themselves, changing the profile so that a very light hypsochromic shift can be seen. A small solvatochromism is also present with respect to the MLCT band of **1**, which has the maximum at 470 nm in DCM, while it is at 450 nm in DMF (Figure 2, inset).

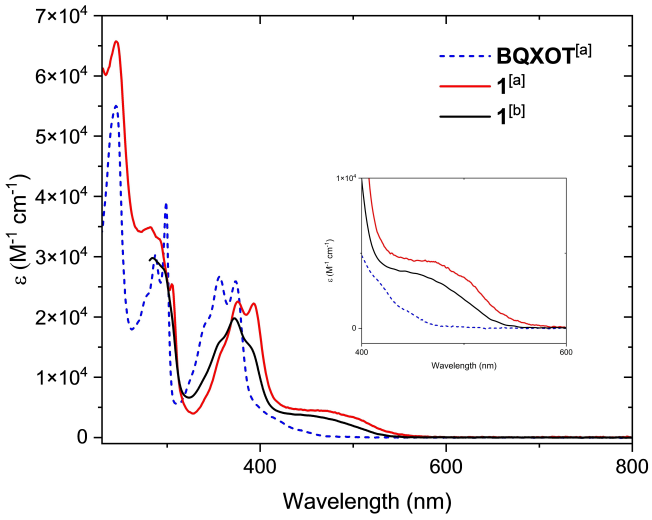

Figure 2. Molar extinction coefficients of the compounds **BQXOT** and **1** in a solution of [a] dichloromethane and [b] *N,N*-dimethylformamide. Inset: Zoom-in of the spectra in the visible range from 400 nm to 600 nm.

The simulated absorption spectra of **1** were investigated employing quantum chemical computations with the TURBOMOLE program package.[16] We optimized the equilibrium geometries using the PBE0-D3(BJ)/def2-TZVP level of theory. For electronic excitations, calculations were performed using the *GW* approximation (correcting the HOMO and LUMO levels) and the Bethe–Salpeter equation (*GW*/BSE).[17] This method shows an excellent agreement with the experimental data (Figure S3), whereas TDDFT and TDDFT with COSMO gave simulated spectra that show slightly less good agreement (Figure S5).

At room temperature, the ligand **BQXOT** emits broadly a yellow light with a maximum at 512 nm. The corresponding excitation spectrum fits the absorption profile very well (Figure S1). The photoluminescent quantum yield was measured using Coumarin 153 in ethanol as the standard[18] and it is 1.5%. The lifetime is 2 ns circa, measured with the time-correlated single photon counting method (TCSPC) (Table 1).

The compound **1** shows no emission in solution, most probably because it deactivates mainly *via* nonradiative pathways (*e.g. via* intersystem crossing (ISC), *vide infra*). Nevertheless, in its solid-state, the Cu(I) complex is moderately emissive with a large unstructured band centered at 697 nm, corresponding to 1.78 eV (Figure S2).

The redox behavior of the non-innocent ligand and its Cu(I) complex, cyclic voltammograms were recorded in a three-electrode cell, using glassy-carbon as working electrode (WE). The samples were measured in 0.1 M supporting electrolyte solutions in DCM and in DMF, with a scan rate of 100 mV/s. The supporting electrolyte was tetrabutylammonium hexafluorophosphate ($TBAPF_6$), and the redox couple ferrocene/ferricenium (Fc/Fc^+) was used as the internal standard (see Table 1). As expected, the ligand does not show any process in the anodic electrochemical window, while it presents two reductions: a quasi-reversible process at −1.95 V and an irreversible

Table 1. Photophysical and electrochemical data of ligand **BQXOT** and Cu(I) complex **1**.

Sample	Solvent	λ_{abs}/nm (ε /M^{-1}cm^{-1})	λ_{em}/nm	Φ[a]	τ[b]/ns	E_{ox}/V	E_{red}/V	ΔE	E_{ox}*/V	E_{red}*/V
BQXOT	**DCM**	340 (18580) 356 (26693) 373 (25878)	512	1.5%	2.1	n.d.	−1.95; −2.52	–	–	>0.47[c]
1	**DCM**	360 (14845) 375 (22495) 393 (22247) 470 (4448)	n.d.[e]	n.d.[e]	n.d.[e]	0.98	−1.57	2.55		
1	**DMF**	356 (15882) 372 (19778) 388 (15297) 450 (3670)	n.d.[e]	n.d.[e]	n.d.[e]	0.89	−1.43; −1.84; −2.24	2.32	≈−1.2[d]	≈0.69[d]

[a] Determined using the relative method, with Coumarin 153 in ethanol as reference [18a]; [b] Measured exciting the sample with NanoLED at 368 nm. [c] Estimated from $E_{red}^* = E_{00} + E_{red}$, and $E_{ox}^* = E_{ox} - E_{00}$, taking as E_{00} energy from the emission in solution for **BQXOT** and [d] from lowest absorption value for **1**. [e] "n.d." means "not detectable" since complex **1** is not emissive in solution.

reduction at −2.52 V, which are a little positively shifted in DMF: −1.84 V and −2.31 V (Figure S6).

Complex **1** shows an oxidation process at 0.98 V in DCM and at 0.89 V in DMF, in both cases it is irreversible and can be assigned to the oxidation Cu(I)/Cu(II). In the negative scans, when the solvent is DCM, only one quasi-reversible reduction process is detectable at −1.57 V. As the electrochemical window of the DMF solvent is larger than the one in DCM in the cathodic scan, several additional quasi-reversible processes appear and can be ascribed mainly to reduction processes localized on the **BQXOT** ligand (Figures S7 and S8). The energy gap between the first oxidation and the first reduction of **1** is 2.55 V in DCM and 2.32 V in DMF. Interestingly, when cyclic voltammetry is recorded under CO_2, instead of an inert atmosphere (Ar), the quasi-reversibility is maintained only for the first reduction process (at −1.43 V). The other reduction signals, which are assigned to the second and the third reduced species $\mathbf{1}^{2-}$ and $\mathbf{1}^{3-}$, respectively, become irreversible with a slight enhancement of the cathodic current and a concomitant shift to higher values (−1.7 V and −2.0 V, respectively). Moreover, a new process appears at −2.8 V (Figure 3). These observations could be indicative of the formation of an unidentified **1**-CO_2 adduct, suggesting that complex **1** might be electrocatalytically active towards CO_2.

Aiming at photocatalytic CO_2 reduction, we chose 1,3-dimethyl-2-phenyl-benzo[d]imidazolidine (BIH) as the sacrificial electron donor. The oxidation of BIH in DMF occurs at −0.18 V versus Fc/Fc^+, as shown in Figure S9. Since complex **1** is not emissive in solution, an approximated estimation of its redox potentials in the excited state was made considering the zero-zero energy level, E_{00}, such as the energy of the lowest absorption wavelength. Nevertheless, the thermodynamics are favorable in case of a reductive quenching of **1*** with BIH, as the calculated difference in the free energy ΔG should be circa −0.85 V. As Stern-Volmer plots were impossible to perform because of the non-emissivity of **1**, we further investigated the reduced forms of the complex **1** by means of UV-Vis spectroelectrochemistry (SEC) and photoirradiating **1** in the presence of BIH. SEC experiments were carried out in DMF (0.1 M $TBAPF_6$), using a platinum grid as the working electrode (Figure 4).

The spectra were recorded while applying a fixed potential. Upon lowering the potential, we observed a decrease in the ligand-centered band, initially peaking at 373 nm and shifting slightly to 376 nm. At the same time, the MLCT band increases and changes its shape, presenting a more structured feature with a peak at 450 nm and two shoulders at 480 and 527 nm. Concomitantly a broad and weak band appears at lower energies, centered at 725 nm. The formation of this new feature started at 0.8 V and reached its final shape at −1.5 V; thus, it was attributed to the first reduced species $\mathbf{1}^-$. Notably, a similar increase of the MLCT band was also observed in a singly reduced Cu(I) complex with an anthraquinone-phenanthroline derivatives as a ligand, recently studied by Mulfort and collaborators.[15a] In that case, the reduced species was assigned to the charge accumulation on one of the carbonyl groups that are present in the ligand. As in our case, a carbonyl group is also present, it is reasonable to ascribe this spectrum to the $\mathbf{1}^-$ species, where the negative charge is on the oxygen and the radical is localized on the aromatic ring. On the other hand, the lower-energy band centered at 725 nm shows similarities to the reduced spectra of a phenazine-phenanthroline-based Cu(I) complex, investigated by Karnahl and Dietzek.[19] As for the phenazine-based heteroleptic Cu(I) complex, this band could be attributed to an intraligand charge transfer (ILCT state) occurring on our diimine ligand **BQXOT**. Further lowering the potential, the absorption intensity diminishes over the entire range, so that the LC peak almost disappears and the three peaks of the MLCT state have almost the same intensity. These

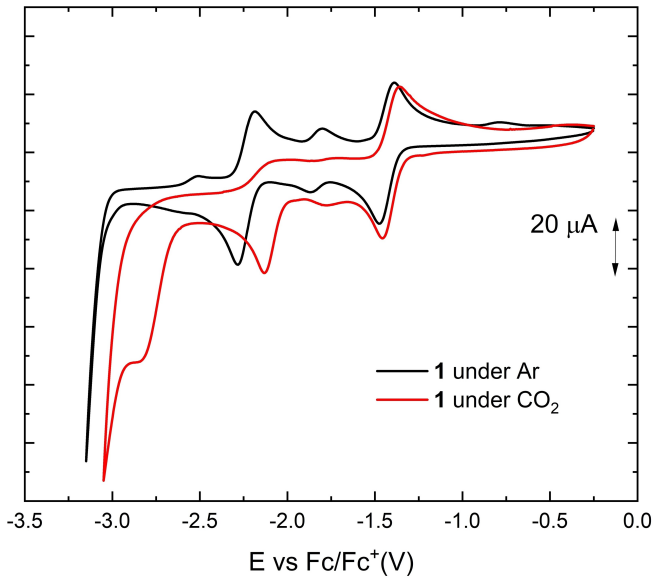

Figure 3. Cyclic voltammetry in DMF (0.1 M $TBAPF_6$) solution under an argon (black curve) and a CO_2 atmosphere (red curve). Scan rate: 100 mV/s.

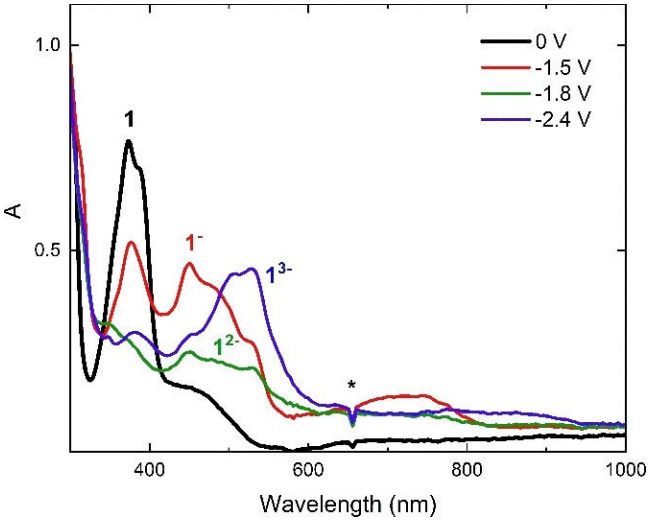

Figure 4. UV-Vis spectroelectrochemistry of complex **1** recorded upon reduction *via* controlled potentials in DMF solution (0.1 M $TBAPF_6$). The shown spectra represent the species at 0 V (black); the first reduced species at −1.5 V (red); the second reduced species (green); and the third reduced species (blue). Asterisk showed the instrumental lamp change.

spectral changes occur when the potential is lowered down to −1.8 V, and as soon as it is further decreased, the MLCT band increases again, maintaining the structured profile, although the peak at 450 nm became a shoulder and the peaks at 503 and 527 nm are the new maxima with almost equal intensity. These observations, corroborated by comparisons with previous literature reports,[15a,20] suggest that the novel heteroleptic Cu(I) complex **1** is able to accumulate up to three charges on the **BQXOT** ligand (Figure S12). When going back to anodic potential, the absorption spectrum of the species in its ground state was completely recovered, as shown in the video provided in the supporting information.

At a later time, we monitored the spectral evolution of **1**, when photoirradiated at 450 nm in the presence of the sacrificial electron donor BIH (Figure S16). First of all, we demonstrated that complex **1** is photostable, as irradiation at 450 nm for more than four hours did not induce any changes in the UV-Vis spectrum or in the ^{1}H NMR (Figure S14 and S15). Subsequently, we prepared a DMF solution 0.1 mM of **1** and 100 mM of BIH. Under an argon atmosphere, after just 30 seconds of blue light irradiation, the absorption has changed, and the spectrum is similar to the one assigned to $\mathbf{1}^-$, obtained *via* SEC (red spectrum in Figure 4). This result indicates that BIH can effectively reduce the excited state of complex **1**, since no spectral changes are observed in the dark. After 20 minutes of irradiation, the new broad band centered at 725 nm disappears and the spectrum resembles one of the species $\mathbf{1}^{2-}$ (green spectrum in Figure 4). We could not observe a similar spectrum for $\mathbf{1}^{3-}$, as after 45 minutes, a new profile with a maximum at around 400 nm was formed. Noteworthy, repeating the experiments with a lower BIH concentration (0.2 mM), only a diminished intensity of the spectrum could be observed, and no spectral features of the reduced forms of the Cu(I) complex could be observed (Figure S17). The irradiated solutions of **1**:BIH (1 : 100) in deuterated DMF under Ar and CO_2 atmosphere were also analyzed by ^{1}H NMR. In the spectra, the disappearance of the signals related to the copper complex in its ground state occurs in more than ten minutes when the solution is under Ar (Figure S19) while it is faster under CO_2, (Figure S18), whereas already after 5 minutes **1** disappears while new signals, most probably related to the reduced species $\mathbf{1}^-$ and/or to $\mathbf{1}^{2-}$, increase their intensity. Indeed, after 1 h of irradiation, the solution is dark red, in agreement with the observations collected during spectroelectrochemistry. Notably, when the solution is left air-equilibrating over a period of 48 h, the ^{1}H NMR showed again the signals of the Cu(I) complex **1**, in addition to some other peaks due to decomposition products (Figure S20). It is important to mention already at this point that BIH, after its first reduction, can release a proton forming an extremely reducing radical: BI·.[21] Thus, it might be that the second electron can be accumulated on the complex by dark electron transfer process.

Aiming at a deeper investigation of the photoinduced electron transfer from the sacrificial electron donor BIH to the excited state of **1**, femtosecond transient absorption experiments were performed upon excitation at 400 nm, in the absence and presence of BIH. Under an inert atmosphere (N_2), the difference in optical density (ΔOD) of a 1 μM DMF solution of **1** showed an intense band with a maximum at 475 nm and a large shoulder at 630 nm circa (Figure S22). Global analysis resulted in three time constants (see Table S2) reminiscent of the analysis by Tahara and coworkers.[22] Accordingly, the first time constant τ_1 can be summarized as structural rearrangements in the excited state (*e.g.* internal conversion, flattening and Jahn-Teller distortion).[23] The subsequent ISC (τ_2) of 12–13 ps in DMF and DCM is slower than the flattening distortion (τ_1) and does not show any significant solvent dependence. In contrast, τ_3 signifies a strong solvent dependence of the triplet state. While the lifetime in DMF is around 360 ps, it considerably exceeds 1 ns in DCM, the latter being consistent with the work of Tahara,[22a] where 41 ns were reported in the same solvent. Adding BIH in a 20-fold excess concentration with respect to **1**, leads to reduced OD and a significant change in the TA spectra. The first band at 475 nm decays much faster with a time constant τ_2 of only 5.4 ps, *i.e.* an acceleration of more than a factor of 2 (see Table S). Additionally, a new band appears at 550 nm within the first picosecond (Figure S23 left). By exploring the ultrafast dynamics of **1** in the presence of a higher concentration of BIH (1 : 100), the observed features are very similar to the previous 1 : 20 ratio (not shown).

When the DMF solution of **1** and BIH (1 : 100) was flushed with CO_2, the main band at 475 nm disappeared and a small ground-state bleaching can be observed around 450 nm. Moreover, the solution became cloudy, revealing the formation of a fine precipitate. Even more interesting the sub-ps dynamic disappears and the global analysis was performed with a biexponential fit with the first time constant attributable to ISC and the second one indicating an increased lifetime in the presence of CO_2. These observations suggest that CO_2 has a role in the ultrafast dynamics of the photoinduced reduced state of the Cu(I) complex. Certainly, this requires further investigations, which go beyond the scope of this study.

Photocatalytic CO_2 Reduction

The investigation of the use of **1** in photo-driven CO_2 catalysis was performed under blue light irradiation at 450 nm. The photocatalytic experiments were prepared by exact dilution of the concentrated solutions of the necessary components, in order to achieve the desired final diluted concentration in a small volume (typical 4 or 5 mL), to minimize the errors. The solutions were transferred to 20 mL glass vials, which were tightly closed with a septum, so that CO_2 (or Ar, for blank experiments) was flushed inside for at least ten minutes. In all experiments, we could detect gaseous products (almost selectively carbon monoxide) *via* collection of aliquots from the head-space and injection in a gas-chromatograph, equipped with two barrier ionization discharge (BID) detectors. We found that the novel complex **1** can act as a photocatalyst for the reduction of CO_2 in the presence of the sacrificial electron donor BIH. The production yield of CO depends strongly not only on the concentration of **1** but also on the ratio between BIH and the PCat. In fact, as shown in Table 2, when for one

Table 2. Photo-driven CO_2 reduction performed in DMF with **1** as PCat.[a]

entry	[1] /mM	[BIH] /mM	CO/μmol	TON[b]
1	0.1	100	1.88	4.69
2	1.0	100	12.11	3.03
3[c]	0.6	20	7.39	2.44
4[c],[d]	0.1	10	1.25	3.13
5[e]	0.1	100	3.40	8.5

[a] 20 mL glass-vials, filled with 4 mL catalytic solution and irradiated for 4 h at 450 nm. [b] TON = # mol of CO/#mol of PCat **1**. [c] Catalytic solution was 5 mL; [d] addition of TEA = 50 mM; [e] 0.2 mM of $Cu(NCCH_3)_4$ BF_4 were added after 2 h of irradiation and the products were analysed after other 2 h.

molecule of PCat there are 1000 molecules of BIH (entry 1), the turnover number (TON) is almost 5, while it decreases to 3 when the ratio is 100 (entry 2) and to 2.4 when the ratio is slightly higher than 33 (entry 3). Usually, the addition of a base such as triethylamine (TEA) favors the reaction,[24] however, no significant improvement could be detected after the addition of 50 mM of TEA (entry 4). Controlled tests were performed in order to verify that the CO production effectively comes from the photo-induced reaction photocatalyzed by **1** in the presence of BIH (Table S3). We could confirm that BIH is necessary to form the reduced catalytic species, as only PCat under a CO_2 atmosphere produced no CO. Also, no carbon monoxide was detected when the reactions were performed under Ar or in the absence of light irradiation (Table S3, entries 2–4). The kinetics were analyzed over four hours. The sigmoidal fitting is shown in Figure 5. The evolution of CO was detected after 30 minutes and reached its maximum after 3 hours. Most probably, we speculated that the catalysis stopped because of a degradation of the catalytic form. In fact, when 0.2 mM of the Cu(I) precursor, $Cu(NCCH_3)_4$ BF_4, tetrakis(acetonitrile)copper(I) tetrafluoroborate, was added after

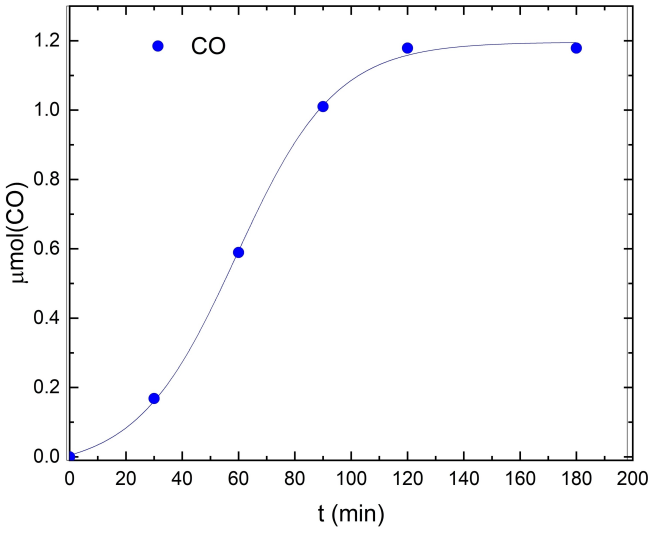

Figure 5. Evolution of the production of CO in the photocatalytic CO_2 reduction. Conditions used: [**1**] = 0.1 mM; [BIH] = 100 mM in DMF, under irradiation at 450 nm. The curve is a sigmoidal fitting.

2 h of irradiation, the photocatalysis continued to rise for other two hours, increasing the production of CO (TON: 8.5), as shown in entry 5 of Table 2. In the control experiment with the Cu(I) precursor as the only copper species in solution, no CO could be detected (entry 6, Table S3). Moreover, the ligand **BQXOT** alone cannot induce any photocatalytic CO_2 reduction (entry 7, Table S3). No production of CO was observed when using another Cu(I) heteroleptic complex, such as $[DPEPhosCu(dmp)]^+$ BF_4^-(where dmp is 2,9-dimethyl-1,10-phenanthroline) (entry 9, Table S3).

To confirm that carbon monoxide is produced from the reduction of CO_2, ^{13}C-labelled carbon dioxide was used. The experiments were performed in NMR tubes, provided with a gas-tight J.-Young valve. ^{13}C-NMR analysis confirmed the presence of the signal at 184.5 ppm, which is ascribed to the ^{13}CO dissolved in deuterated DMF. This signal is not present when non-labelled CO_2 was used (Figure S25).

Interestingly, in the catalytic solution with high BIH content (1 : 1000) under CO_2, fine white particles could be seen. If these particles were filtered off by a 0.2 μm filter, the catalysis stopped. Therefore, a non-filtered photocatalytic solution was investigated by scanning electron microscopy (SEM) after 4 h of irradiation. As shown in the supporting information file, the SEM analyses revealed that there are microparticles of circa 1.5 μm size and below, which are mainly of an organic nature and are not purely metallic nanoparticles (Figures S27–S29). In fact, the energy-dispersive X-ray analysis (EDX) of these particles revealed that they are primarily composed of carbon atoms. Thus, we propose that these organic microparticles might result from an aggregation product, induced by the negatively charged complex, the BIH and CO_2 molecule.

Therefore, by removing these aggregates by filtration, the catalytic species is removed, and the CO_2 reduction stops. Furthermore, it was observed that the particles were redissolved in the solution in the dark. Further investigations to understand in more detail the structure of the particles are currently ongoing. Although at the present stage, we cannot provide deep mechanistic explanations, we proposed a catalytic cycle of photocatalyst **1** in Scheme S1.

Interestingly, we performed bimolecular photo-induced CO_2 reduction experiments using complex **1** as a mere catalyst, while the photosensitization occurs via the employment of $[Ru(bpy)_3]^{2+}$ $(PF_6^-)_2$. The results, shown in Table S4, are a further indication that this complex can act also as a catalyst in combination with another photosensitizer.

Besides the extraordinary properties of **1** as photocatalyst, we explored its employment as photosensitizer, combined with 5,10,15,20-tetrakis(pentafluorophenyl)-21*H*,23*H*-porphyrin iron(III) chloride as catalyst (**Fe**-CAT, Figure 6), (Table 3). Porphyrins are very well-employed catalyst in photo- and electrocatalytic CO_2 reduction,[5a,b,25] and the chosen Fe(III) porphyrin was previously used in some studies related to electrocatalytic CO_2 reduction,[26] and in photocatalytic CO_2 reduction, employing $Ru(bpy)_3^{2+}$ as PS.[27] To the best of our knowledge, its use in visible-light-driven CO_2 reduction experiments in combination with an earth-abundant photosensitizer has never been reported so far. The reduction potentials of **Fe**-CAT showed that

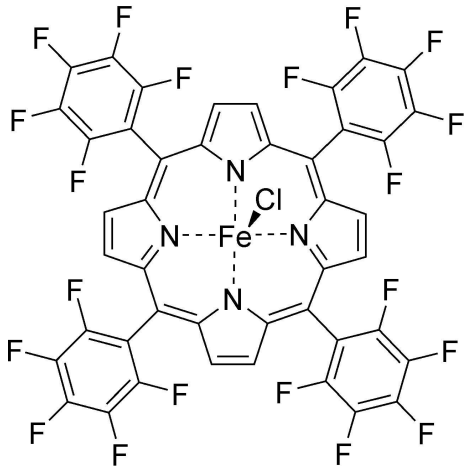

Figure 6. Chemical structure of the Fe(III) porphyrin used in this work.

the porphyrin can be reduced by the $\mathbf{1}^-$ species, with a thermodynamically favored free energy value ($\Delta G < -1$ V), see Figure S26.

A first screening was done with the PS:BIH ratio of 1:40, to have enough reduced species in solution able to reduce **Fe**-CAT and, at the same time, to avoid an overwhelming CO-production by **1**. The photocatalysis was explored also in acetonitrile (ACN) and in propylene carbonate (PC), since it was shown that the electrocatalysis of **Fe**-CAT is more efficient in those solvents.[26b] As shown in entries 1–4 of Table 3, the photo-driven CO_2 reduction in ACN and PC produced almost the same amount of carbon monoxide. The copper complex **1** also exhibits a photocatalytic activity in these solvents, although much lower than that in DMF. At this stage, it is not possible to know if the catalytic cycles involving solely **1** as PCat and the system **1** + **Fe**-CAT can coexist or if the latter is prevalent. In Table 3 we assumed that the total CO amount is produced from the PS and CAT system in the calculation of TON. However, if we consider that a certain amount of CO comes from the PCat cycle, this contribution is certainly overestimated if we take the values of the photocatalyses with only **1** present. Nevertheless, subtracting the CO values produced without Fe-CAT (entries 2 and 4, Table 3) to the respective values, a TON_{CAT}, referred to the activity due to the **Fe**-CAT, of 113 in ACN and 92 in PC, which are still higher than the benchmark results. In DMF, since the concentration of the catalyst was doubled in respect to the previous performed experiments, the CO produced was 9 μmol (entry 5, Table 3). Thus, subtracting the values obtained with only **1** as PCat (entry 3, Table 2), the CO produced by the photocatalytic system **1** + **Fe**-Cat is 1.6 μmol, which corresponds to a TON_{CAT} of 40. These results are quite interesting, as the TON obtained in ACN, PC and DMF follow the same trends observed in electrocatalysis.[26a,b] Nevertheless, it must be stressed that in photocatalytic experiments solvent effects involve not only the catalyst but also the photosensitizer. Thus, we examined further the photocatalysis in DMF.

Increasing the concentration of the photosensitizer **1** to 1 mM and that one of the electron donor to 100 mM, a remarkable CO production of about 18 μM could be observed, corresponding to a TON of more than 800 (entries 6 and 7, Table 3). Interestingly, as we cannot distinguish if CO is produced preferentially from the PS + Cat or the PCat pathway, we estimated the TONcat values by subtracting the relative CO amounts produced in the PCat pathway (Table 2). Even so, the PS + Cat system composed of **1** and **Fe**-Cat developed CO abundantly with a TON up to 285. These results are remarkable, especially when comparing the CO production of the Fe(III)-Cat in other photocatalytic systems with Ru-based PS, where the TON was up to 170 after four hours.[27]

Conclusions

A newly synthesized mononuclear copper(I) complex demonstrates its potential as both a photosensitizer and a photocatalyst for CO_2 reduction. These appealing properties, attributed to the non-innocent ligand 1-ethyl-3-(1′-benzyl-1′,2′,3′-triazol-4′-yl)-benzo[g]quinoxalin-2-one, were thoroughly characterized through photophysical and electrochemical analyses both in DCM and DMF as well as by theoretical calculations.

Table 3. Photodriven CO_2 reduction performed in DMF with **1** as PS.[a]

entry	[**Fe**-CAT] / mM	[BIH] / mM	Solvent	CO/μmol	TON_{PS}[b]	TON_{CAT}[c]
1	0.005	20	ACN	2.67	–	134
2	0	20	ACN	0.4	0.2	–
3	0.005	20	PC	2.69	–	134
4	0	20	PC	0.8	0.42	–
5	0.01	20	DMF	9.0	–	226
6[d]	0.01	100	DMF	18.2	–	454
7[d]	0.005	100	DMF	17.8	–	891
8[e]	0.01	20	DMF	0.13	–	3.2
9[f]	0.01	–	DMF	0.26	–	6.2

[a] 20 mL glass-vials, filled with 4 mL catalytic solution and irradiated for 4 h at 450 nm. PS concentration is 0.5 mM unless specified. Solvents used are ACN = CH_3CN; PC = propylene carbonate and DMF = *N*,*N*-dimethylformamide; [b] TON_{PS} = # mol of CO/#mol of PS **1**.; [c] TON_{CAT} = # mol of CO/#mol of **Fe**-CAT. [d] PS concentration is 1 mM. [e] no PS. [f] no PS and triethylamine (TEA) 100 mM as the electron donor.

Cyclic voltammetry studies conducted in DMF under a CO_2 atmosphere revealed its catalytic potential. Further investigations of the photostability, coupled with spectral changes resulting from reduction, were conducted *via* UV-Vis spectroelectrochemistry and photoinduced electron transfer from the electron donor BIH. The remarkable similarity between the absorption spectra obtained through these two methods conclusively validates the reduction quenching of the excited state of the copper complex **1** by the sacrificial electron donor BIH. The hypothesis of a charge transfer involving the excited state of the complex was further corroborated by femtosecond transient absorption spectroscopy. The benzoquinoxalinone unit serves as the electron reservoir of the copper complex, enabling the necessary charge accumulation for the interaction with carbon dioxide. Indeed, the photocatalytic experiments using **1** as PCat were performed, yielding selectively carbon monoxide, with a TON up to 4.6, after two hours. This result is excellent, since it is the first case of a mononuclear Cu(I)-based complex behaving as photocatalyst in CO_2 reduction. The concentration of BIH also plays an important role. Hypotheses of the mechanism could be promoted thanks to additional analyses with SEM and ^{1}H NMR. Further investigations are currently ongoing, aiming at a deeper understanding of the photocatalytic process. Moreover, we demonstrated that, under different conditions, the Cu(I) complex could also act as a photosensitizer, when combined with a known iron-porphyrin catalyst, reaching TON(CO) of 891. Finally, this novel complex exhibits fascinating properties, enabling it to function in photo-driven CO_2 reduction with diverse roles.

Experimental Section

Experimental Details and General Remarks

All starting materials and solvents were purchased from commercial suppliers and used as received unless otherwise noted. Fe(III)-Cat 5,10,15,20-tetrakis(pentafluorophenyl)-21*H*,23*H*-porphyrin iron(III) chloride was purchased from Sigma-Aldrich. For the synthesis of the diketone **3** (2-oxo-4-(triisopropylsilyl)but-3-ynoate) a previously published procedure was followed.[28]

Synthesis of 3-((triisopropylsilyl)ethynyl)benzo[g]quinoxalin-2(1*H*)-one (4)

2,3-diaminonaphthalene (**2**) (0. 253 g, 1.6 mmol, 1.00 equiv.) was reacted with methyl 2-oxo-4-(triisopropylsilyl)but-3-ynoate (**3**) (0.670 g, 2.5 mmol, 1.50 equiv.) into a 50 mL mixture of ethanol and acetic acid (7 : 3), at 80° for 15 h. Water was added afterwards and the organic products were extracted with dichloromethane (three times). The collected organic phase was washed with water and brine, dried over Na_2SO_4 and filtered. The solvent was reduced under vacuum. The product was obtained clean as a yellow solid without the need of further purification. (0.460 g, 1.22 mmol) Yield: 76 %. ^{1}H NMR (400 MHz, $CDCl_3$) δ = 11.59 (s, 1H), 8.34 (s, 1H), 7.91 (d, J = 8.3 Hz, 1H), 7.77 (d, J = 8.4 Hz, 1H), 7.55 (s, 1H), 7.51 (ddd, J = 8.2, 6.7, 1.2 Hz, 1H), 7.41 (ddd, J = 8.1, 6.6, 1.1 Hz, 1H), 1.19 (d, J = 4.3 Hz, 21H) ppm. ^{13}C NMR (101 MHz, $CDCl_3$) δ = 155.95, 143.51, 134.49, 132.62, 130.65, 129.33, 129.25, 128.96, 128.60, 126.93, 125.51, 111.71, 103.23, 102.14, 18.92, 11.50 ppm. HRMS (ESI, $[M]^+$) *m/z* ($C_{23}H_{28}N_2OSi$): 377.2049 (calc.), 377.2039 (found).

Synthesis of 1-ethyl-3-((triisopropylsilyl)ethynyl)benzo[g]quinoxalin-2(1*H*)-one (5)

3-((triisopropylsilyl)ethynyl)benzo[g]quinoxalin-2(1*H*)-one (**4**) (0.390 g, 1.036 mmol, 1.00 equiv.) and K_2CO_3 (0.286 g, 2.071 mmol, 2.00 equiv.) were dissolved in anhydrous DMF (5 mL). After 30 minutes, iodoethane (170 uL, 323 mg, 2.071 mmol, 2.00 equiv.) was added and the reaction was left under stirring at 50 °C for two hours. Water was added afterwards, and the organic products were extracted with dichloromethane (three times). The collected organic phase was washed with brine, dried over Na_2SO_4 and filtered. The solvent was reduced under vacuum. The desired compound, the regioisomer obtained in larger quantity, was isolated by a silica gel column chromatography using Cy/EtOAc (70 : 30) as eluent to obtain a yellow solid with a yield of 81 % (405 mg, 0.84 mmol). ^{1}H NMR (400 MHz, $CDCl_3$) δ = 8.41 (s, 1H), 7.99–7.94 (m, 1H), 7.90 (dd, J = 8.5, 1.0 Hz, 1H), 7.60 (d, J = 3.5 Hz, 1H), 7.59–7.55 (m, 1H), 7.48 (ddd, J = 8.2, 6.8, 1.2 Hz, 1H), 4.41 (q, J = 7.2 Hz, 2H), 1.46 (t, J = 7.2 Hz, 3H), 1.27–1.18 (m, 21H) ppm. ^{13}C NMR (101 MHz, $CDCl_3$) δ = 153.51, 143.00, 134.25, 132.84, 130.19, 130.16, 129.70, 128.79, 128.37, 127.20, 125.45, 109.83, 102.51, 101.82, 37.62, 18.71, 12.11, 11.32 ppm. HRMS (ESI) *m/z* ($C_{25}H_{32}N_2OSi$): 405.2362 (calc.), 405. 2353 (found).

Synthesis of 1-ethyl-3-ethynylbenzo[g]quinoxalin-2(1*H*)-one (6)

1-ethyl-3-((triisopropylsilyl)ethynyl)benzo[g]quinoxalin-2(1*H*)-one (**5**) (0.260 g, 0.64 mmol, 1.00 equiv.) was dissolved in dry THF (20 mL). Then a THF solution of TBAF (1 M, 0.64 mL, 0.64 mmol, 1.00 equiv.) was added slowly at −78 °C. After ten minutes of stirring, an ammonium chloride solution (20 mL) was added for the quenching and the organic products were extracted with EtOAc (three times). The collected organic phase was then washed with brine, dried over Na_2SO_4 and filtered. The solvent was removed under vacuum. The crude was purified adding an excess of pentane to a concentrated dichloromethane solution, to obtain a yellow solid as precipitate. (0.119 g, 0.48 mmol) Yield: 75 %. ^{1}H NMR (400 MHz, $CDCl_3$) δ = 8.31 (s, 1H), 7.89 (d, J = 8.3 Hz, 1H), 7.85–7.80 (m, 1H), 7.56–7.49 (m, 2H), 7.42 (ddd, J = 8.1, 6.7, 1.2 Hz, 1H), 4.33 (q, J = 7.2 Hz, 2H), 3.52 (s, 1H), 1.38 (t, J = 7.2 Hz, 3H) ppm.

Synthesis of 3-(1′-benzyl-1′*H*-1′,2′,3′-triazol-4′-yl)-1-ethylbenzo[g]quinoxalin-2(1*H*)-one (BQXOT)

1-ethyl-3-ethynylbenzo[g]quinoxalin-2(1*H*)-one (**6**) (0.120 g, 0.48 mmol, 1.00 equiv.) was dissolved in a solution of ethanol and water (7 : 3). Then the other reactants were added in the following order: sodium ascorbate (0.053 g, 0.27 mmol, 0.56 equiv.), copper sulphate penta-hydrate (0.024 g, 0.10 mmol, 0.20 equiv.), sodium carbonate (0.023 g, 0.28 mmol, 0.59 equiv.), benzylazide (0.064 g, 0.48 mmol, 1.00 equiv.). The reaction mixture was left under stirring for two days. After this period time, a solution of NH_4OH (10 %) was added and the organic products were extracted with dichloromethane (three times). The combined organic phases were washed with water and brine, dried over Na_2SO_4 and filtered. The solvent was removed under vacuum. The product was purified by silica gel column chromatography using DCM/MeOH (95 : 5) as eluent. The product was obtained as a yellow powder. (0.170 g, 0.45 mmol) Yield: 92 %. ^{1}H NMR (400 MHz, $CDCl_3$) δ = 8.75 (d, J = 18.1 Hz, 2H), 8.04 (d, J = 8.3 Hz, 1H), 7.94 (d, J = 8.4 Hz, 1H), 7.71 (s, 1H), 7.60 (ddd, J = 8.2, 6.8, 1.3 Hz, 1H), 7.52 (ddd, J = 8.1, 6.8, 1.3 Hz, 1H),

7.44–7.33 (m, 5H), 5.68 (s, 2H), 4.48 (q, J = 7.2 Hz, 2H), 1.50 (t, J = 7.2 Hz, 3H) ppm. ^{13}C NMR (126 MHz, CD_2Cl_2) δ = 159.07, 159.02, 158.97, 152.67, 144.78, 144.77, 142.82, 134.91, 134.84, 134.80, 134.77, 134.13, 132.59, 132.08, 132.02, 131.96, 131.17, 131.07, 130.92, 130.77, 130.48, 130.34, 130.21, 130.18, 130.05, 129.88, 129.62, 129.48, 129.37, 129.33, 129.29, 128.82, 128.78, 128.75, 128.64, 128.57, 128.50, 127.41, 126.04, 125.61, 125.59, 125.57, 123.78, 123.65, 123.53, 120.81, 111.23, 55.79, 38.43, 30.08, 12.42 ppm. MS (EI) *m/z* $C_{23}H_{19}N_5O$: 382.256 $[M+H]^+$.

Synthesis of the Cu(I) Complex (1)

Following a previously published procedure,[10a] the copper precursor, $Cu(CH_3CN)_4BF_4$ (0.163 g, 0.52 mmol, 1.00 equiv.) and the dichelating phoshine ligand DPEPhos (0.279 g, 0.52 mmol, 1.00 equiv.) were dissolved in a solution of dry dichloromethane, under an Ar atmosphere. After 30 minutes of reaction, the diimine ligand **BQXOT** (0.198 g, 0.52 mmol, 1.00 equiv.) was added to the solution and the reaction mixture was left under stirring for four hours. Lastly, the solvent was removed under reduced pressure. The crude product was dissolved in a minimum amount of dichloromethane and crystallized by a slow diffusion of cyclohexane. The product was obtained as red crystals with a yield of 79% (0.440 g, 0.41 mmol). ^{1}H NMR (400 MHz, CD_2Cl_2) δ = 8.66 (s, 1H), 8.37 (s, 1H), 7.89 (d, J = 8.4 Hz, 1H), 7.76 (s, 1H), 7.60–7.51 (m, 5H), 7.43–7.24 (m, 14H), 7.11 (dt, J = 8.2, 2.8 Hz, 2H), 7.04 (t, J = 7.8 Hz, 3H), 6.96 (t, J = 7.5 Hz, 2H), 6.90–6.79 (m, 6H), 6.70 (q, J = 6.6, 6.1 Hz, 4H), 5.69 (s, 2H), 4.48 (q, J = 7.1 Hz, 2H), 1.50 (t, J = 7.1 Hz, 3H) ppm. ^{13}C NMR (126 MHz, CD_2Cl_2) δ = 159.07, 159.02, 158.97, 152.67, 144.78, 144.77, 142.82, 134.91, 134.84, 134.80, 134.77, 134.13, 132.59, 132.08, 132.02, 131.96, 131.17, 131.07, 130.92, 130.77, 130.48, 130.34, 130.21, 130.18, 130.05, 129.88, 129.62, 129.48, 129.37, 129.33, 129.29, 128.82, 128.78, 128.75, 128.64, 128.57, 128.50, 127.41, 126.04, 125.61, 125.59, 125.57, 123.78, 123.65, 123.53, 120.81, 111.23, 55.79, 38.43, 30.08, 12.42 ppm. HRMS (ESI) *m/z* ($C_{59}H_{47}CuN_5O_2P_2^+$): 982.2501 (calc.), 982.2481 (found). Elemental analysis $[C_{59}H_{47}BCuF_4N_5O_2P_2]$: C = 66.21, H = 4.43, N = 6.54 (calc.); C = 65.87, H = 4.45, N = 6.64 (found).

UV-vis absorption spectra were acquired in spectroscopically grade solvents (DCM, DMF) at specific concentrations. The instruments used for this scope are: Perkin Elmer Lambda 750 double-beam UV/Vis-NIR spectrometer and a SEC2020 spectrometer from ALS-Japan (detector range: 200–1025 nm).

Photoluminescence was recorded on a Horiba FluoroMax 4 spectrofluorometer from HORIBA Scientific. Lifetimes were determined by TCSPC (Time-correlated single photon counting) using a DeltaTime kit (DeltaHub and DeltaDiode controller). NanoLED 370 was used for the excitation. Quantum yield was evaluated with the relative method, using Coumarin 153 dye as fluorescent standard in aerated ethanol.

Transient absorption measurements were performed in 1 mm cuvettes from Starna (suprasil quartz). A more detailed description of the experimental setup can be found elsewhere.[29] In addition, the cuvettes were closed with a septum and flushed with N_2 for roughly 15 min. For recordings in the UV/Vis-range, the output of a Ti/sapphire laser (Astrella, Coherent, 800 nm 1 kHz, 35 fs, 7 mJ) was split into pump and probe pulse. The pump-pulses were generated via frequency doubling in a BBO-crystal. Prior to generating the white light continuum with a CaF_2-crystal (350–750 nm) the pulses propagated a computer-controlled delay stage (Thorlabs) before entering the sample equipped with a micro-stirring unit. Afterwards it was split into two segments and dispersed by prisms to monitor the pump-induced changes via two CCD-cameras (Linescan Series2000, 512 pixels, SI detector, Entwicklungsbüro Stresing). Transient spectra were further processed with in house written software (LabView – recording, Mathematica – group velocity compensation, MatLab – global analysis).

Electrochemistry

Cyclic Voltammetry was recorded on a potentiostat/galvanostat "Gamry Interface 1010B". The three-electrodes electrochemical cell was equipped with a glassy-carbon (GC) disc (2 mm diameter) as working electrode; a platinum wire as auxiliary electrode and a silver wire as quasi-reference electrode. Thus, ferrocene was added at the end of each measurement as an internal standard.[30] A small tube allowed argon to flow inside the cell. Electrochemical solutions contained 0.1 M of tetrabutylammonium hexafluorophosphate. Analyte concentration ranged from 2 mM to 10 mM. Scan rates were 100 mV/s unless otherwise noted.

Photocatalysis

Typical photocatalytic reactions were performed in 20 mL glass vials, closed *via* a screw-aluminum cap with a rubber septum. The photocatalytic solutions were prepared dissolving the components in 4 mL of solvent (typically: DMF, ACN, PC). Usually, the (photo)catalysts were previously dissolved in concentrated solutions (from 1 to 5 mM), from which the necessary aliquots were collected and diluted in the final photocatalytic solution. The reactions were irradiated in a photoreactor (LZC-IC2 from Luzchem), equipped with two LED lamps at 453 nm (5 W). The generated gaseous products were quantified by gas-chromatography, *via* a Shimadzu GC-2030 instrument, equipped with two barrier ionization discharge detectors (BID). Details regarding the columns and the methods of detection can be found in our previous publication.[9e] Other possible C1-products were not detected by ^{1}H NMR or mass analyses. The total photon flux of the lamps used was determined using potassium ferrioxalate as a standard actinometer,[31] and it is 1.3×10^{-7} E/s. Thus, the quantum yield of the reactions was calculated as follows:

$$\mathbf{\Phi}(\%) = \frac{\#\ \boldsymbol{CO\ molecules}}{\#\ \boldsymbol{absorbed\ photons}\ \times (1-10^{-A})} \times 100$$

Where # indicates "number", A is the initial absorbance of the photocatalytic solution of the tests at the irradiation wavelength. The apparent quantum yield of the reactions using **1** as the photocatalyst is 0.8%, while Φ is 1.2% when **1** is used as the photosensitizer (with Fe(III) porphyrin as the catalyst).

Experiments were done also with ^{13}C-labeled CO_2. This gas was generated in a separated vial containing $Na^{13}CO_3$ and gently adding a concentrated solution of H_2SO_4. The generated gas was transferred via cannula to the photocatalytic system, previously deaerated with three cycles of freeze-pump-thaw.

Supporting Information

Electronic supporting information contains: details of the single crystal molecular structure analysis, additional UV-Vis absorption and emission spectra; calculated absorption spectra; transient absorption spectra and data; cyclic voltammograms; spectroelectrochemical measurements; monitoring of photo-irradiation and photocatalytic experiments; a table with other molecular photocatalysts for CO_2 reduction and the ^{1}H and ^{13}C

NMR spectra of the synthesized compounds. The authors have cited additional references within the Supporting Information[12c,32] Deposition Number CCDC-2301141 for **1** contains the supplementary crystallographic data for this paper . These data are provided free of charge by the joint Cambridge Crystallographic Data Centre and Fachinformationszentrum Karlsruhe Access Structures service.

Acknowledgements

The authors thank the financial support of the German Research Foundation (DFG), for the past SFB/TRR 88 Project. Bizzarri also thanks the German Scholar Organization and the Klaus Tschira Boost Fund. We thank Dr. Zibat (KIT) for performing the SEM measurements. Open Access funding enabled and organized by Projekt DEAL Open Access funding enabled and organized by Projekt DEAL.

Conflict of Interests

The authors declare no conflict of interest.

Data Availability Statement

The data that support the findings of this study are available in the supplementary material of this article.

Keywords: CO_2 reduction · Cu(I) Photocatalyst · Fe(III) porphyrin · visible-light · electron accumulation

[1] J. Barber, P. D. Tran, *J.R. Soc. Interface* **2013**, *10*, 20120984.
[2] E. Olivieri, J. M. Gallagher, A. Betts, T. W. Mrad, D. A. Leigh, *Nat. Synth.* **2022**, *1*, 189–189
[3] a) Y. Yamazaki, H. Takeda, O. Ishitani, *J. Photochem. Photobiol. C: Photochem. Rev.* **2015**, *25*, 106–137; b) S. Berardi, S. Drouet, L. Francàs, C. Gimbert-Suriñach, M. Guttentag, C. Richmond, T. Stoll, A. Llobet, *Chem. Soc. Rev.* **2014**, *43*, 7501–7519.
[4] a) H. Yuan, J. Du, M. Ming, Y. Chen, L. Jiang, Z. Han, *J. Am. Chem. Soc.* **2022**, *144*, 4305–4309; b) Q. Lei, H. Yuan, J. Du, M. Ming, S. Yang, Y. Chen, J. Lei, Z. Han, *Nat. Commun.* **2023**, *14*, 1087.
[5] a) E. Boutin, L. Merakeb, B. Ma, B. Boudy, M. Wang, J. Bonin, E. Anxolabéhère-Mallart, M. Robert, *Chem. Soc. Rev.* **2020**, *49*, 5772–5809; b) L. Zou, R. Sa, H. Lv, H. Zhong, R. Wang, *ChemSusChem* **2020**, *13*, 6124–6140; c) Y. Wei, L. Chen, H. Chen, L. Cai, G. Tan, Y. Qiu, Q. Xiang, G. Chen, T.-C. Lau, M. Robert, *Angew. Chem. Int. Ed.* **2022**, *61*, e202116832.
[6] N. Elgrishi, M. B. Chambers, X. Wang, M. Fontecave, *Chem. Soc. Rev.* **2017**, *46*, 761–796.
[7] L. Wang, *Catalysts* **2022**, *12*, 919.
[8] a) H. Takeda, A. Kobayashi, K. Tsuge, *Coord. Chem. Rev.* **2022**, *470*, 214700; b) G. A. Álvarez, E. Mejía, in *Photochemistry and Photophysics of Coordination Compounds* (Eds.: R. Ameta, A. K. Rai, J. P. Bhatt, S. Bhardwaj, S. C. Ameta), Elsevier, **2023**, pp. 293–340; c) P. A. Forero Cortés, M. Marx, M. Trose, M. Beller, *Chem Catalysis* **2021**, *1*, 298–338; d) J. Beaudelot, S. Oger, S. Peruško, T.-A. Phan, T. Teunens, C. Moucheron, G. Evano, *Chem. Rev.* **2022**.
[9] a) H. Takeda, K. Ohashi, A. Sekine, O. Ishitani, *J. Am. Chem. Soc.* **2016**, *138*, 4354–4357; b) F. Doettinger, M. Obermeier, V. Caliskanyürek, L. E. Burmeister, C. Kleeberg, M. Karnahl, M. Schwalbe, S. Tschierlei, *ChemCatChem* **2023**, *15*, e202300452; c) R. S. Khnayzer, C. E. McCusker, B. S. Olaiya, F. N. Castellano, *J. Am. Chem. Soc.* **2013**, *135*, 14068–14070; d) J.-W. Wang, X. Zhang, L. Velasco, M. Karnahl, Z. Li, Z.-M. Luo, Y. Huang, J. Yu, W. Hu, X. Zhang, K. Yamauchi, K. Sakai, D. Moonshiram, G. Ouyang, *JACS Au* **2023**, *3*, 1984–1997; e) L.-L. Gracia, E. Barani, J. Braun, A. B. Carter, O. Fuhr, A. K. Powell, K. Fink, C. Bizzarri, *ChemCatChem* **2022**, *14*, e202201163; f) F. Doettinger, C. Kleeberg, C. Queffélec, S. Tschierlei, Y. Pellegrin, M. Karnahl, *Catalysis Science, Technology* **2023**, *13*, 4092–4106; g) H. Takeda, Y. Monma, H. Sugiyama, H. Uekusa, O. Ishitani, *Front. Chem.* **2019**, *7*; h) L.-L. Gracia, P. Henkel, O. Fuhr, C. Bizzarri, *Beilstein J. Org. Chem.* **2023**, *19*, 1766–1775; i) J.-W. Wang, Z. Li, Z.-M. Luo, Y. Huang, F. Ma, S. Kupfer, G. Ouyang, *Proc. Natl. Acad. Sci. USA* **2023**, *120*, e2221219120.
[10] a) C. Bruschi, X. Gui, N. Salaeh-arae, T. Barchi, O. Fuhr, S. Lebedkin, W. Klopper, C. Bizzarri, *Eur. J. Inorg. Chem.* **2021**, *2021*, 4074–4084; b) L.-L. Gracia, L. Luci, C. Bruschi, L. Sambri, P. Weis, O. Fuhr, C. Bizzarri, *Chem. Eur. J.* **2020**, *26*, 9929–9937; c) C. Bruschi, X. Gui, O. Fuhr, W. Klopper, C. Bizzarri, *Dalton Trans.* **2023**, *52*, 7809–7818.
[11] a) S. K. Lee, M. Kondo, M. Okamura, T. Enomoto, G. Nakamura, S. Masaoka, *J. Am. Chem. Soc.* **2018**, *140*, 16899–16903; b) H. Hori, F. P. A. Johnson, K. Koike, O. Ishitani, T. Ibusuki, *J. Photochem. Photobiol. A* **1996**, *96*, 171–174; c) A. J. Huckaba, E. A. Sharpe, J. H. Delcamp, *Inorg. Chem.* **2016**, *55*, 682–690; d) A. Maurin, C.-O. Ng, L. Chen, T.-C. Lau, M. Robert, C.-C. Ko, *Dalton Trans.* **2016**, *45*, 14524–14529; e) S. Sato, T. Morikawa, *ChemPhotoChem* **2018**, *2*, 207–212; f) S. Sato, T. Morikawa, T. Kajino, O. Ishitani, *Angew. Chem.* **2013**, *125*, 1022–1026; g) A. Genoni, D. N. Chirdon, M. Boniolo, A. Sartorel, S. Bernhard, M. Bonchio, *ACS Catal.* **2017**, *7*, 154–160; h) S. Das, R. R. Rodrigues, R. W. Lamb, F. Qu, E. Reinheimer, C. M. Boudreaux, C. E. Webster, J. H. Delcamp, E. T. Papish, *Inorg. Chem.* **2019**, *58*, 8012–8020; i) J. Hawecker, J.-M. Lehn, R. Ziessel, *Helv. Chim. Acta* **1986**, *69*, 1990–2012; j) C. A. Carpenter, P. Brogdon, L. E. McNamara, G. S. Tschumper, N. I. Hammer, J. H. Delcamp, in *Inorganics*, *Vol. 6*, **2018**; k) T. Ishizuka, A. Hosokawa, T. Kawanishi, H. Kotani, Y. Zhi, T. Kojima, *J. Am. Chem. Soc.* **2023**, *145*, 23196–23204.
[12] a) J. Grodkowski, D. Behar, P. Neta, P. Hambright, *J. Phys. Chem. A* **1997**, *101*, 248–254; b) D. Behar, T. Dhanasekaran, P. Neta, C. M. Hosten, D. Ejeh, P. Hambright, E. Fujita, *J. Phys. Chem. A* **1998**, *102*, 2870–2877; c) H. Rao, J. Bonin, M. Robert, *Chem. Commun.* **2017**, *53*, 2830–2833.
[13] H. Yuan, B. Cheng, J. Lei, L. Jiang, Z. Han, *Nat. Commun.* **2021**, *12*, 1835.
[14] a) R. Angamuthu, P. Byers, M. Lutz, A. L. Spek, E. Bouwman, *Science* **2010**, *327*, 313–315; b) R. J. Haines, R. E. Wittrig, C. P. Kubiak, *Inorg. Chem.* **1994**, *33*, 4723–4728.
[15] a) Z.-L. Xie, N. Gupta, J. Niklas, O. G. Poluektov, V. M. Lynch, K. D. Glusac, K. L. Mulfort, *Chem. Sci.* **2023**, *14*, 10219–10235; b) G. Li, H. Phan, T. S. Herng, T. Y. Gopalakrishna, C. Liu, W. Zeng, J. Ding, J. Wu, *Angew. Chem. Int. Ed.* **2017**, *56*, 5012–5016.
[16] a.d. o. U. O. K. A. TURBOMOLE V7.7 2022, –. Forschungszentrum Karlsruhe GmbH, s. a. f. TURBOMOLE GmbH, https://www.turbomole.org., *Vol. 2022*, V7.7 ed.
[17] a) K. Krause, W. Klopper, *J. Comput. Chem.* **2017**, *38*, 383–388; b) C. Holzer, W. Klopper, *J. Chem. Phys.* **2019**, *150*, 204116.
[18] a) G. Jones, W. R. Jackson, C. Y. Choi, W. R. Bergmark, *J. Phys. Chem.* **1985**, *89*, 294–300; b) A. Brouwer, *Pure Appl. Chem.* **2011**, *83*, 2213–2228.
[19] Y. Zhang, L. Zedler, M. Karnahl, B. Dietzek, *Phys. Chem. Chem. Phys.* **2019**, *21*, 10716–10725.
[20] a) R. Giereth, I. Reim, W. Frey, H. Junge, S. Tschierlei, M. Karnahl, *Sustain. Energy Fuels* **2019**, *3*, 692–700; b) M. A. Argüello Cordero, P. J. Boden, M. Rentschler, P. Di Martino-Fumo, W. Frey, Y. Yang, M. Gerhards, M. Karnahl, S. Lochbrunner, S. Tschierlei, *Inorg. Chem.* **2022**, *61*, 214–226; c) M. Schulz, N. Hagmeyer, F. Wehmeyer, G. Lowe, M. Rosenkranz, B. Seidler, A. Popov, C. Streb, J. G. Vos, B. Dietzek, *J. Am. Chem. Soc.* **2020**, *142*, 15722–15728.
[21] Y. Tamaki, K. Koike, T. Morimoto, O. Ishitani, *J. Catal.* **2013**, *304*, 22–28.
[22] a) M. Iwamura, S. Takeuchi, T. Tahara, *J. Am. Chem. Soc.* **2007**, *129*, 5248–5256; b) M. Iwamura, H. Watanabe, K. Ishii, S. Takeuchi, T. Tahara, *J. Am. Chem. Soc.* **2011**, *133*, 7728–7736.
[23] a) M. Iwamura, S. Takeuchi, T. Tahara, *Acc. Chem. Res.* **2015**, *48*, 782–791; b) S. Garakyaraghi, E. O. Danilov, C. E. McCusker, F. N. Castellano, *J. Phys. Chem. A* **2015**, *119*, 3181–3193.
[24] Y. Pellegrin, F. Odobel, *C. R. Chim.* **2017**, *20*, 283–295.
[25] a) J. Bonin, A. Maurin, M. Robert, *Coord. Chem. Rev.* **2017**, *334*, 184–198; b) E. Anxolabéhère-Mallart, J. Bonin, C. Fave, M. Robert, *Dalton Trans.* **2019**, *48*, 5869–5878.
[26] a) I. Azcarate, C. Costentin, M. Robert, J.-M. Savéant, *J. Am. Chem. Soc.* **2016**, *138*, 16639–16644; b) B. Zhao, H. Lei, N. Wang, G. Xu, W. Zhang, R.

Cao, *Chem. Eur. J.* **2020**, *26*, 4007–4012; c) E. A. Mohamed, Z. N. Zahran, Y. Naruta, *J. Mater. Chem. A* **2021**, *9*, 18213–18221.
[27] E. Pugliese, P. Gotico, I. Wehrung, B. Boitrel, A. Quaranta, M.-H. Ha-Thi, T. Pino, M. Sircoglou, W. Leibl, Z. Halime, A. Aukauloo, *Angew. Chem. Int. Ed.* **2022**, *61*, e202117530.
[28] T. Karasawa, R. Oriez, N. Kumagai, M. Shibasaki, *J. Am. Chem. Soc.* **2018**, *140*, 12290–12295.
[29] A. P. Veenstra, P. Rauthe, J. Czekner, J. Hauns, A.-N. Unterreiner, M. M. Kappes, *J. Phys. Chem. A* **2022**, *126*, 8930–8938.
[30] a) R. R. Gagne, C. A. Koval, G. C. Lisensky, *Inorg. Chem.* **1980**, *19*, 2854–2855; b) G. Gritzner, J. Kuta, *Pure Appl. Chem.* **1984**, *56*, 461–466.
[31] C. G. Hatchard, C. A. Parker, E. J. Bowen, *Proc. R. Soc. Lond. Ser. A Math Phys. Sci.* **1956**, *235*, 518–536..
[32] a) O. V. Dolomanov, L. J. Bourhis, R. J. Gildea, J. A. K. Howard, H. Puschmann, *J. Appl. Crystallogr.* **2009**, *42*, 339–341; b) G. Sheldrick, *Acta Crystallogr. Sect. A* **2015**, *71*, 3–8; c) G. Sheldrick, *Acta Crystallogr. Sect. C* **2015**, *71*, 3–8.

Manuscript received: February 24, 2024
Accepted manuscript online: May 14, 2024
Version of record online: June 25, 2024